Chemical Engineering Journal 306 (2016) 86–98

Contents lists available at ScienceDirect

Chemical Engineering Journal

journal homepage: www.elsevier.com/locate/cej

VOCs abatement in adiabatic monolithic reactors: Heat effects, transport limitations and design considerations

M.L. Rodríguez [a,*], L.E. Cadús [a], D.O. Borio [b]

[a] INTEQUI (UNLS/CONICET), Chacabuco y Pedernera, San Luis, Argentina
[b] PLAPIQUI (UNS/CONICET), Camino La Carrindanga km. 7, Bahía Blanca, Argentina

HIGHLIGHTS

- The role of inlet temperature to control VOC emissions with low energy requirements is elucidated.
- Impact of internal mass transport limitations and external mass and heat transport limitations are analysed.
- Higher VOC concentrations increase heat effects and accelerate the reaction rates.
- Poor interfacial areas contribute to VOC abatement.
- Pseudohomogeneous models can significantly over – or underestimate the outlet VOC concentration.

GRAPHICAL ABSTRACT

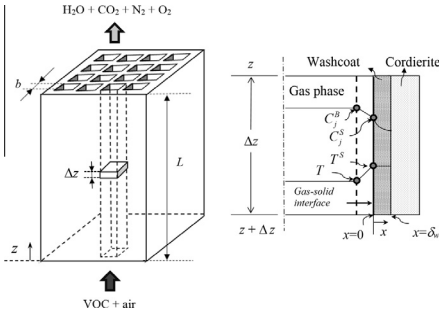

ARTICLE INFO

Article history:
Received 6 December 2015
Received in revised form 19 April 2016
Accepted 12 May 2016
Available online 2 June 2016

Keywords:
Catalytic oxidation
VOC
Monolithic reactor
Heterogeneous model
Mass transport limitations
Heat transport limitations

ABSTRACT

A simulation study of a monolithic reactor for the catalytic oxidation of Volatile Organic Compounds (VOC) over a Mn-Cu mixed oxide catalyst is presented. A heterogeneous 1D mathematical model is selected to describe the performance of the reactor under adiabatic and steady-state operation. Internal (washcoat) mass transport limitations and external (gas-solid) mass and heat transport limitations in the reactor are taken into account.

Proper quantification and analysis of both, internal and external resistances contribute to design and operate the reactor under conditions that favour VOC abatement.

The influence of the heat effects and different operating variables and design parameters on the reactor performance are analysed, aiming to meet environmental standards of VOC emissions with the lowest preheating energy requirements.

1. Introduction

Emission control of hazardous air pollutants, including Volatile Organic Compounds (VOCs), is one of the priorities for environmental catalysis because of its many harmful effects on health and the environment [1].

VOCs are mostly generated by chemical and petrochemical industries. These emissions should be treated to reduce their concentration to the permitted levels currently established by global environmental standards. The European Commission sets an emission limit value (ELV) of 20 mg C/Nm^3 in a stream discharged into the atmosphere [2].

Catalytic oxidation is a particularly suitable technology for treating large flows of low VOC concentrations [1,3].

Considerable efforts have been directed towards obtaining suitable catalysts for catalytic oxidation of VOCs [4–6]. It has been

* Corresponding author.
E-mail address: mlrodri@unsl.edu.ar (M.L. Rodríguez).

http://dx.doi.org/10.1016/j.cej.2016.05.055
1385-8947/

Notation

a_v	gas-solid interfacial area, m^2/m^3
A_l	lateral area, m^2, calculated as $A_L = 4(b - 2\delta_w)CNL$
A_o	open frontal area, m^2, calculated as $A_o = (b - 2\delta_w)^2 CN$
A_T	transversal area, m^2, calculated as $A_r = b^2 CN$
b	channel width = height, mm
C_j	concentration of j component, mol_j/m^3 or mg C/m^3
$C_{s,j}$	concentration of j component in the solid phase, mol_j/m^3 or mg C/m^3
$C^S_{s,j}$	concentration of j component at surface of the solid phase, mol_j/m^3 or mg C/m^3
C^*_{VOC}	emission limit value of VOC, mg C/m^3
CN	channels number, dimensionless
Cp_j	specific heat of j component, kJ/(kmol K)
$D_{e,j}$	effective diffusion coefficient for j component, m^2/s
E_i	activation energy of i reaction, J/ mol
$GHSV$	gas-hourly space velocity, 1/h
h_e	convective heat transfer coefficient, J/(s m^2 K)
$k_{g,j}$	convective mass transfer coefficient from gas to solid interface, $m^3_f/(m^2$ s)
$k_{ref,1}$	kinetic constant of reaction 1, 1/s
$k_{ref,2}$	kinetic constant of reaction 2, mol/(m^3 s)
Kc_j	adsorption constant of j component, m^3/mol
L	channel length, m
m_w	catalyst mass, g
P	pressure, atm
q_{gen}	heat generation rate, J/(m^3 h), calculated as $q_{gen} = \eta_{1,int} r^S_1(-\Delta H_{r1}) + \eta_{2,int} r^S_2(-\Delta H_{r2})$
Q_0	volumetric feed flow rate, N m^3/h
r_i	reaction rate of i reaction, i = 1, 2, mol/(m^3_w s)
r^B_i	reaction rate of i reaction at gas phase, i = 1, 2, mol/(m^3_w s)
r^{eff}_i	effective reaction rate of i reaction, i = 1, 2, mol/(m^3_w s)
r^S_i	reaction rate of i reaction at gas-solid interface, i = 1, 2, mol/(m^3_w s)
R	universal gas constant, J/(mol K)
T	gas phase temperature, °C
T^S	solid phase temperature, °C
$T_{0,min}$	minimum inlet temperature, °C
u_s	average gas velocity, m/s
V_g	gas volume, m^3
V_w	washcoat volume, m^3
x	transversal coordinate, m
y_j	molar fraction of j component, dimensionless
z	axial coordinate, m
C	carbon
C_2H_5OH	ethanol
C_2H_4O	acetaldehyde
CO_2	carbon dioxide
H_2O	water
LHHW	Langmuir-Hinshelwood
O_2	oxygen

Greek letters

δ_w	washcoat thickness, μm
ΔH^o_{ri}	heat of i reaction at standard conditions, J/mol
ΔH_{ri}	heat of i reaction, J/mol
ΔT	total temperature gradient (inlet-outlet) in the gas phase, °C
$\Delta T_{s\text{-}g}$	interfacial temperature gradient, °C
$\Delta T_{s\text{-}g,max}$	maximum interfacial temperature gradient, °C
$\eta_{i,ext}$	external effectiveness factor of i reaction, dimensionless
$\eta_{i,int}$	internal effectiveness factor of i reaction, dimensionless
$\overline{\eta}_{i,ext}$	axially averaged external effectiveness factor of i reaction, dimensionless
$\overline{\eta}_{i,\mathrm{int}}$	axially averaged internal effectiveness factor of i reaction, dimensionless
ρ_w	washcoat density, kg/m^3

Subscripts

Ac	acetaldehyde
Et	ethanol
ext	external
i	i reaction
int	internal
j	j component
max	maximum
min	minimum
ref	reference
s-g	solid-gas interface
VOC	volatile organic compound
w	washcoat
0	at the axial coordinate z = 0

Superscripts

B	at bulk gas phase
eff	effective
S	at solid surface
*	reference condition

demonstrated that Mn–Cu mixed oxide catalysts are highly active at moderate temperatures for the catalytic oxidation of a wide variety of VOCs [7]. Catalysts have a finite life in terms of activity, and exposure to high temperature over time reduces the catalytic activity [4,8]. Additionally, for large flow rates, the preheating of the gaseous stream to achieve the required temperature levels that guarantee full VOCs conversion, produces a significant operative cost [9]. Recuperative catalytic conversion is a promising choice to preheat the gaseous stream, in which the thermal energy in the effluent gas is exchanged with the influent [10] but is not always suitable when the stream presents temporal emissions patterns.

An accurate determination and setting of the minimal inlet temperature of the gaseous stream according to its flow rate and VOC inlet concentration as an anticipative control strategy, would contribute to reaching the ELV of VOCs emissions with minimum economic loss.

In the last three decades, the success of monoliths as converters of engine emissions has encouraged researchers to improve other gas phase reactions by using monolithic catalysts and reactors [11]. The major advantages of this design are low pressure drops under high fluid throughputs leading to an energy-efficient operation, short diffusion path in the catalyst and high external surface area, among others [11,12]. All these advantages become monoliths particularly appropriate for catalytic combustion [12,13].

Detailed modelling and simulation play a very important role in the designs of these systems [14–17]. Since catalytic combustion reactions are extremely fast, both inter-phase and intra-phase transport limitations are likely to be significant and have to be properly considered to analyse a reactor performance. Numerous

theoretical studies have been conducted with the aim of understanding the effect of these resistances. Internal diffusion limitation could be significant when temperature is high (>430–530 °C) even with very thin washcoat thickness [15,18]. Geometrical parameters also have a relevant influence on internal diffusion limitation, Leung et al. [19] and Kolaczkowski and Serbetcioglu [15] studied CO oxidation over noble metals based catalyst systems. They demonstrated that the internal diffusion is strongly affected by the catalyst accumulation in the corners of the channels. A similar conclusion was reached by Tomašić and Gomzi [20] when they performed 2-D simulation of NO decomposition in a catalytic monolith reactor. Hayes et al. [21], investigated the influence of washcoat and channel shape on the mass transfer concluding that the internal diffusion affects the magnitude of the external mass transfer resistance. The washcoat thickness, the channel radius, including its non-uniformity around the channel, and the angular diffusion in the washcoat caused by variable thickness are the three factors that determine the rates of mass transfer.

Holmgren and Andersson [22] observed that for CO oxidation, external mass transfer became the controlling step at temperatures as low as 300 °C. In addition the combination of external mass and heat transfer could make the effect even stronger [15], which could not be neglected during kinetics study or scale-up design.

Design variables such as opening and cross-sectional shape of the monolith channels also have a significant influence on the heat transfer properties. Kolodziej and Lojewska [23] studied the efficiencies of different units of short-channel structures built of differently shaped (triangular, parallel plates and square) for combustion of air pollutants in terms of the mass and heat transport and the reaction kinetics. Groppi et al. [24] demonstrated that the light-off position inside the reactor is anticipated when increasing the channels diameter and is also associated with square channel cross sections. As a general fact, monoliths with worse transport properties exhibit better light-off characteristics [25,26].

In this work, we present a theoretical study of a monolithic reactor for the catalytic oxidation of ethanol over a Mn-Cu mixed oxide catalyst using Langmuir-Hinshelwood kinetic expressions. A heterogeneous 1D mathematical model is selected to describe the performance of a pilot scale reactor of square channel section under adiabatic and steady-state operation.

The study explores and evaluates the relative importance of internal (washcoat) mass transport limitations and external (gas-solid) mass and heat transport limitations in the reactor with the aim of defining the conditions that meet environmental standards of VOC emissions with the lowest preheating energy requirements under different operating scenarios. There are also explored geometric conditions that increase external temperature gradients and favour VOCs abatement.

From the results is also possible determine the range of operation conditions where simplified models (isothermal heterogeneous model and adiabatic pseudohomogenous model) can significantly over- or underestimate the outlet VOC concentration, leading respectively, to undesirable situations of excessive preheating of the air stream to meet VOC emissions specifications or, conversely, to risky conditions of incomplete VOC abatement.

2. Mathematical model

2.1. Model equations

Fig. 1a shows the schematic representation of the design under study. A stream of ethanol diluted in air enters the ceramic monolithic reactor. Channels of square section are impregnated with the Mn–Cu mixed oxide catalyst [27]. Fig. 1b illustrates the mass and heat transfer resistances considered in a differential control volume.

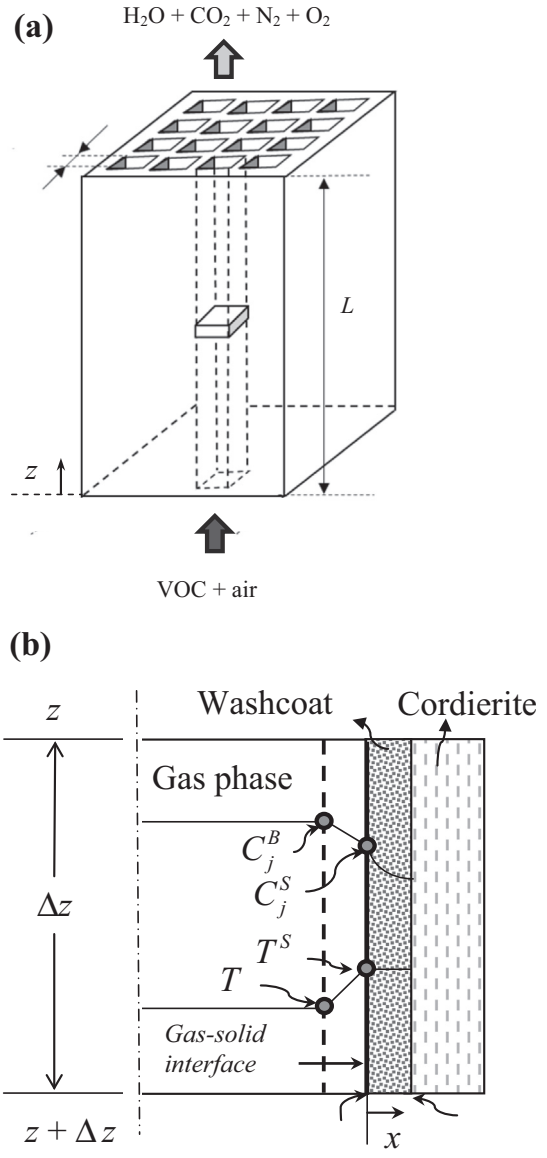

Fig. 1. (a) Schematic representation of the monolithic reactor. (b) Representation of the mass and heat transfer resistances considered in a differential control volume.

A heterogeneous 1-D mathematical model is proposed to simulate the adiabatic and steady state operation of the monolith reactor, based on the following hypotheses:

(a) Fully developed laminar flow through the channels is assumed, leading to low pressure drops and nearly isobaric conditions.
(b) Concentration and temperature variations in radial direction (plug flow) are neglected [28].
(c) Heat losses to the surrounding are neglected.
(d) Axial dispersion of heat and mass is neglected (axial mass and heat Peclet numbers are much higher than 50) [28].
(e) Internal and external mass transfer diffusional limitations are considered as well as external heat transfer resistances.
(f) Isothermal conditions in the catalyst layer are assumed from the evaluation of Biot number [29] and Prater number [30], both values are much less than one.

(g) Inside the channel the flow is unidirectional
(h) A single channel is assumed to be representative of the whole reactor: the velocity distribution is uniform among the channels, the catalyst is equally distributed and there is no radial heat loss [16].

By assuming that the distribution of the washcoat is uniform around the perimeter of the cell, the catalyst layer may then be modelled as a slab of thickness δ_w.

The catalytic combustion of ethanol is evaluated by means of the kinetic model proposed by Campesi et al. [31]. Two series reactions are considered: partial oxidation of ethanol to acetaldehyde and combustion of acetaldehyde (see Table 1). Table 2 lists the kinetic parameters and the standard heats of reactions 1 and 2. Since there are two reactions involved, the mass balances corresponding to ethanol and acetaldehyde are enough to know the extent of reaction 1 (ε_1) and 2 (ε_2). The concentrations of the remaining species CO_2, O_2, N_2 and H_2O are obtained from the molar balances as function of the parameters ε_1 and ε_2 [32].

Under the stated hypotheses, the reactor is represented by the following equations:

Gas phase

Mass balances

$$\frac{dC_{Et}}{dz} = -\frac{V_w}{u_s V_g}\eta_{1,\text{int}} r_1^S \tag{3}$$

$$\frac{dC_{Ac}}{dz} = \frac{V_w}{u_s V_g}\left(\eta_{1,\text{int}} r_1^S - \eta_{2,\text{int}} r_2^S\right) \tag{4}$$

$$\eta_{i,\text{int}} = \frac{\int_0^{V_w} r_i(C_{s,j})dV_w}{V_w r_i(C_j^S)} = \frac{r_i^{eff}}{r_i^S} \tag{5}$$

Heat balance

$$\frac{dT}{dz} = \frac{V_w}{u_s V_g}\frac{\eta_{1,\text{int}} r_1^S(-\Delta H_{r1}) + \eta_{2,\text{int}} r_2^S(-\Delta H_{r2})}{\sum_{j=1}^{6} Cp_j C_j} \tag{6}$$

Inlet conditions:

At z=0:

$$C_{Et} = C_{0Et}, \quad C_{Ac} = C_{0Ac}, \quad T = T_0 \tag{7}$$

Table 1
Reaction system and kinetic expressions [31].

Reaction system	Kinetic expressions	
$C_2H_6O + (1/2)O_2 \rightarrow C_2H_4O + H_2O$	$r_1 = \frac{k_{ref,1}\exp\left[-(E_1/R)(1/T-1/T_{ref})\right]C_{Et}}{1+Kc_{Et}C_{Et}+Kc_{Ac}C_{Ac}}$	(1)
$C_2H_4O + (5/2)O_2 \rightarrow 2CO_2 + 2H_2O$	$r_2 = \frac{k_{ref,2}\exp\left[-(E_2/R)(1/T-1/T_{ref})\right]Kc_A}{1+Kc_{Et}C_{Et}+Kc_{Ac}C_{Ac}}$	(2)

Table 2
Kinetic parameters [31] and standard heats of reactions.

Parameter	Optimal value and confidence interval
$k_{ref,1}$	$(1.81 \pm 0.3) \times 10^3$ 1/s
$k_{ref,2}$	$(1.81 \pm 0.26) \times 10^{-1}$ mol/(s m^3)
E_1	$(1.10 \pm 0.04) \times 10^5$ J/mol
E_2	$(1.69 \pm 0.09) \times 10^5$ J/mol
Kc_{Et}	~0
Kc_{Ac}	$(6.75 \pm 1.26) \times 10^2$ m^3/mol
$-\Delta H_{r1}^o$	1.73×10^5 J/mol
$-\Delta H_{r2}^o$	1.10×10^6 J/ mol

Solid phase

Mass balances (washcoat)

$$D_{e,Et}\frac{d^2C_{s,Et}}{dx^2} = -\frac{V_w}{V_g} r_1(C_{s,j}) \tag{8}$$

$$D_{e,Ac}\frac{d^2C_{s,Ac}}{dx^2} = \frac{V_w}{V_g}(r_1(C_{s,j}) - r_2(C_{s,j})) \tag{9}$$

Boundary conditions:

At x = 0 (gas-solid interphase):

$$k_{g,j}(C_j - C_{s,j}^S) = -D_{e,j}\left(\frac{dC_{s,j}}{dx}\right)\Big|_{x=0} \tag{10}$$

At x = δ_w (washcoat-cordierite surface):

$$\frac{dC_{s,j}}{dx} = 0 \text{ with } j = Et, Ac \tag{11}$$

Heat balance

$$a_v h_e(T^S - T) = \eta_{1,\text{int}} r_1^S(-\Delta H_{r1}) + \eta_{2,\text{int}} r_2^S(-\Delta H_{r2}) \tag{12}$$

Physical parameters of the catalyst (mean pore radius, washcoat porosity and tortuosity factor) [33] and physical and thermodynamic properties of the components are extracted from the open literature [32,34].

The convective mass and heat transfer coefficients are obtained from the Nusselt expression applicable to square-channel structured reactors proposed by Hawthorn [35]. Molecular binary diffusivity is calculated following Fuller, Schettler and Giddings's [36] semi empirical equation. Molecular mixed diffusivity for diluted systems, Knudsen diffusivity and effective diffusivity are calculated according to Froment and Bischoff's [37] guidelines.

2.2. Numerical solution

The differential equations for the gas phase are integrated using the Gear method [38]. The differential equations for the washcoat are discretized by means of second order finite differences, using a grid of equally spaced points. For each axial position, the nonlinear algebraic equations generated by the interior grid points are solved through a Quasi-Newton algorithm.

3. Results and discussion

3.1. Influence of inlet temperature (T_0)

Fig. 2 illustrates the influence of the inlet temperature on the outlet concentration of the carbonaceous species involved in the reactions: ethanol, acetaldehyde and carbon dioxide, as well as the total outlet VOC concentration (ethanol + acetaldehyde). These results are obtained at both constant ethanol inlet concentration (C_{0Et} = 1000 mg C/m^3) and constant gas hourly space velocity ($GHSV = 3.04 \times 10^5$ 1/h). *GHSV* is calculated as the ratio between the volumetric flow rate at normal conditions and the total volume of the catalyst. The main operative conditions and design parameters are summarized in Table 3.

The behaviour of the ethanol concentration is monotonically in decrease with inlet temperature while carbon dioxide concentration displays a continuous raise due to the evolution of reaction 2. Acetaldehyde concentration exhibits the typical behaviour of an intermediary species, this is, firstly it presents an ascending zone at temperatures at which is mainly produced, reaching a maximum at T_0 = 169 °C, beyond which the concentration shows a descending zone because the acetaldehyde consumption is favoured by high temperatures.

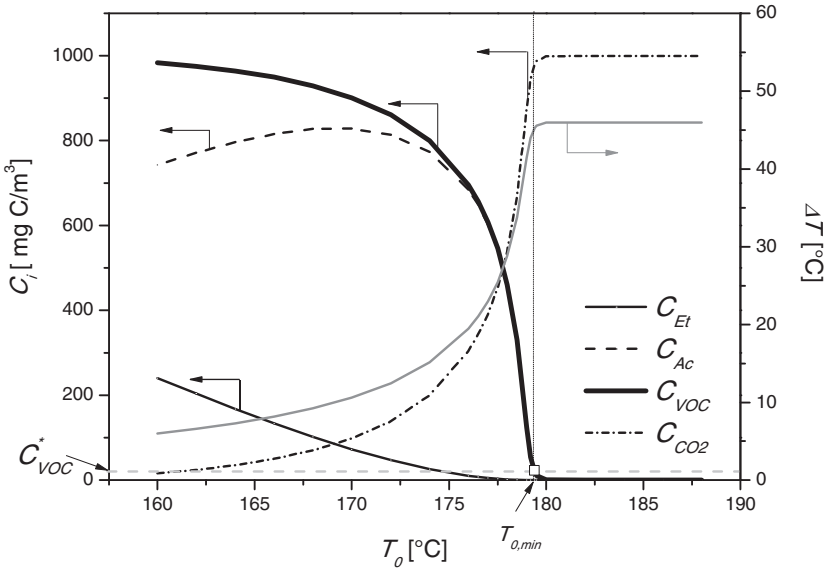

Fig. 2. Influence of the inlet temperature, on both the outlet concentration of the carbonaceous species (left ordinate axis) and total temperature gradient in the gas phase (right ordinate axis) for $GHSV = 3.04 \times 10^5$ 1/h, $b = 1.115$ mm, $\delta_w = 20$ μm, $CN = 13{,}950$ and $L = 10$ cm.

Table 3
Operative and geometrical parameters.

Parameter	Value
Channel length, L	0.10 m
Channel width = height, b	1115 μm
Cell density	400 cpsi
Channels number, CN	13,950
Monolithic material	cordierite ($2MgO{\cdot}2Al_2O_3{\cdot}5SiO_2$)
Support	Nyacol
Catalytic material	Mn–Cu
Washcoat thickness, δ_w	20 μm
Washcoat density, ρ_w	4030 kg/m^3
Washcoat mass, m_w	665 g
Inlet temperature, T_0	160–200 °C
Inlet pressure, P_0	1 atm
Volumetric feed flow rate, Q_0	37.2 m^3/h
Gas-hourly space velocity, $GHSV$	3.04×10^5 1/h
Inlet VOC concentration, C_{0Et}	50–1500 mg C/m^3

The total VOC concentration curve presents a continuous decrease with T_0, overlapping with the acetaldehyde curve at temperatures at which ethanol concentration has been almost totally consumed.

To accomplish VOC emissions standards, outlet VOC concentrations must be lower than 20 mg C/m^3. This limit concentration value is called C^*_{VOC} and the minimum inlet temperature that achieves C^*_{VOC} is called $T_{0,\min}$ (see Fig. 2).

Fig. 2 also shows the total temperature gradient (inlet-outlet) in the gas phase (ΔT) at the right ordinate axis. ΔT increases with the inlet temperature in accordance with the increase in the VOC conversions (higher heat generation). When the total VOC conversion is achieved, ΔT reaches 46 °C, the value of the adiabatic temperature rise for these inlet conditions.

Fig. 3 presents ignition curves for three different inlet ethanol concentration values ($C_{0Et} = 500$, 1000 and 1500 mg C/m^3) at constant space velocity ($GHSV = 3.04 \times 10^5$ 1/h).

The increase in C_{0Et} leads to more significant thermal effects within the reactor. ΔT increases from 24 °C (for $C_{0Et} =$ 500 mg C/m^3) to almost 70 °C (for $C_{0Et} = 1500$ mg C/m^3).

As C_{0Et} increases, the intensification of the heat effects causes faster consumption of VOCs. As a consequence, the ignition curves become sharper and the value of $T_{0,\min}$ decreases. This diminution in the minimum inlet temperature to satisfy the emission standards would be even more pronounced in metallic monoliths, because of the heat conduction towards the reactor inlet occurring through the solid phase. This heat feedback contributes to the reaction ignition and has not been taken into account in the present work, due to ceramic monoliths with low thermal conductivities are considered.

Fig. 4 shows the minimum inlet temperatures to ensure the environmental specifications (20 mg C/m^3) at different inlet ethanol concentrations, for the same space velocity ($GHSV = 3.04 \times 10^5$ 1/h) and design parameters ($b = 1.115$ mm, $\delta_w = 20$ μm, $CN = 13950$, $L = 10$ cm). The right ordinate axis exhibits both the reactor temperature rise (ΔT) and the maximum temperature drop over the external film along the reactor (or maximum interfacial temperature gradient) ($\Delta T_{s\text{-}g,max}$).

At low values of C_{0Et} the heat effects are mild, and higher inlet temperatures are needed to achieve C^*_{VOC}, i.e., higher $T_{0,min}$ are necessary to reach the higher required VOC conversions. For the case of $C_{0Et} = 450$ mg C/m^3, the inlet temperature to reduce the involved VOCs to the desirable value reaches its maximum value, i.e, $T_{0,\min}$ - ~ 181.4 °C. Further increments of C_{0Et} leads to more significant temperature gradients in the monolith, it can be noticed the increase of both, ΔT and $\Delta T_{s\text{-}g,max}$. These higher thermal effects accelerate the effective reaction rates (r_1^{eff} and r_2^{eff}), as a consequence lower $T_{0,min}$ are required to meet the outlet specification.

Maximum difference between bulk and surface temperatures ($\Delta T_{s\text{-}g,max}$) may be considered significant for C_{0Et} higher than 1000 mg C/m^3, and for 1500 mg/m^3 the interfacial thermal gradient rises up to 12 °C.

Four different operative conditions are shown in Fig. 4: points A, B, C and D. Four C_{0Et} are selected ($C_{0Et} = 150$, 500, 1000 and 1500 mg C/m^3) at the same inlet temperature ($T_0 = 180$ °C). The representation demonstrates that for the lowest C_{0Et} value (150 mg C/m^3, condition A), an inlet temperature of 180 °C is high enough to meet the specification. For an intermediate C_{0Et} value (500 mg C/m^3, condition B) the temperature is not enough to reduce the VOC content. For the two highest C_{0Et} values (1000 and 1500 mg C/m^3, conditions C and D, respectively) T_0 enables meet the standards once again.

Axial concentration profiles of ethanol and acetaldehyde for these four operating conditions are exhibited in Fig. 5a. Ethanol shows more pronounced decreasing profiles as C_{0Et} is increased,

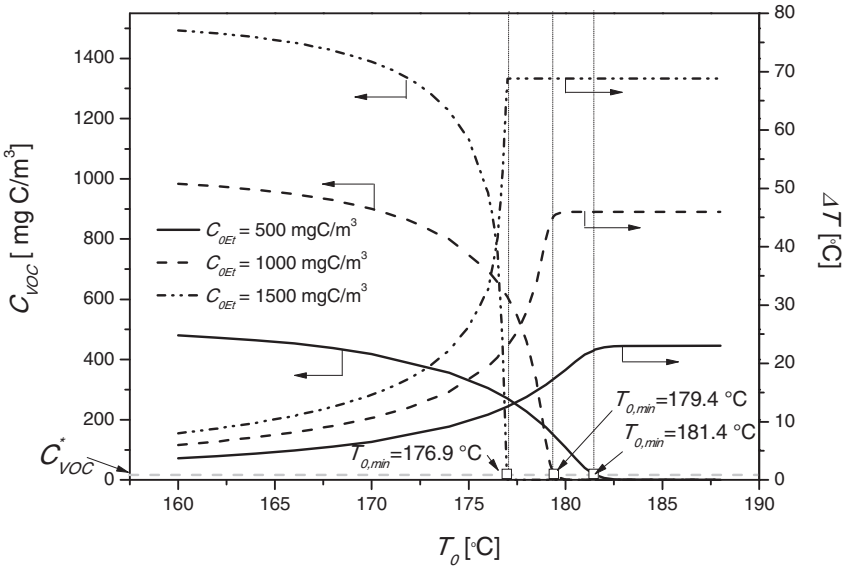

Fig. 3. Influence of the inlet temperature, on both, the outlet concentration of the carbonaceous species (left ordinate axis) and total temperature gradient in the gas phase (right ordinate axis) for the same conditions of Fig. 2 at three level of C_{0Et}.

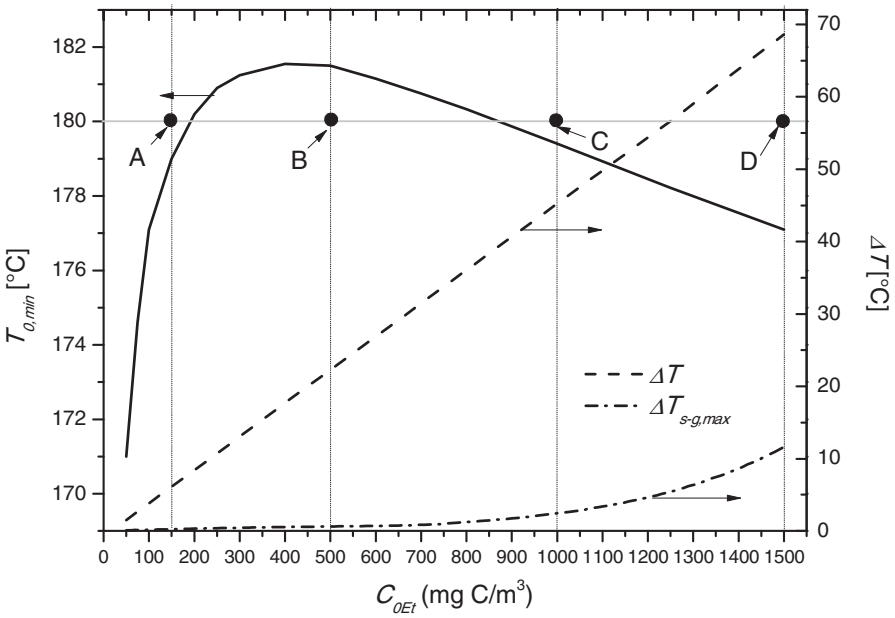

Fig. 4. $T_{0,min}$ for different C_{0Et} (left ordinate axis). Total temperature gradient in the gas phase (ΔT) and maximum temperature drop over the film inside the reactor ($\Delta T_{s\text{-}g,max}$) (right ordinate axis).

and for all the cases ethanol is completely removed. The acetaldehyde curves present the expected maximum, which is more relevant as C_{0Et} increases. As described above, for the low C_{0Et} value (150 mg C/m^3, condition A) it is possible to reach the standard, i.e. the acetaldehyde concentration (C_{Ac}) is lower than 20 mg C/m^3 at the reactor outlet. This does not occur for C_{0Et} = 500 mg C/m^3 (condition B) being C_{Ac} at z = 10 cm clearly higher than 20 mg C/m^3. Finally, for the two highest values of C_{0Et}, $C_{Ac} \sim 0$ at z = 10 cm (conditions C and D). For C_{0Et} = 1000 mg C/m^3 the complete VOC abatement is achieved at $z \sim 9.5$ cm, while for C_{0Et} = 1500 mg c/m^3 a complete VOC elimination is reached at $z \sim 7.6$ cm due to further contribution of the thermal effects. Fig. 5b displays the corresponding axial temperature profiles in the gas and solid phases. The total temperature rises are more relevant as C_{0Et} increases: ΔT is 6 °C for C_{0Et} = 150 mg C/m^3 and ΔT is almost 70 °C for C_{0Et} = 1500 mg C/m^3. The axial profiles of the interfacial temperature differences, $\Delta T_{s\text{-}g}$, are presented in Fig. 5c. The maximum temperature gradient over the external film is around 3 °C for C_{0Et} = 1000 mg C/m^3 and almost 14 °C for C_{0Et} = 1500 mg C/m^3.

In Fig. 6, the curves of $T_{0,min}$ obtained from the adiabatic heterogeneous model and an idealized isothermal heterogeneous model are compared.

For the isothermal model, the mass balances in gas and solid phase remain unchanged (Eqs. (3)–(5) and (8)–(11)), however the heat effects of the reaction rates are neglected ($\Delta H_{ri} \sim 0$) and the axial gas phase temperature is constant and equal to the solid phase temperature.

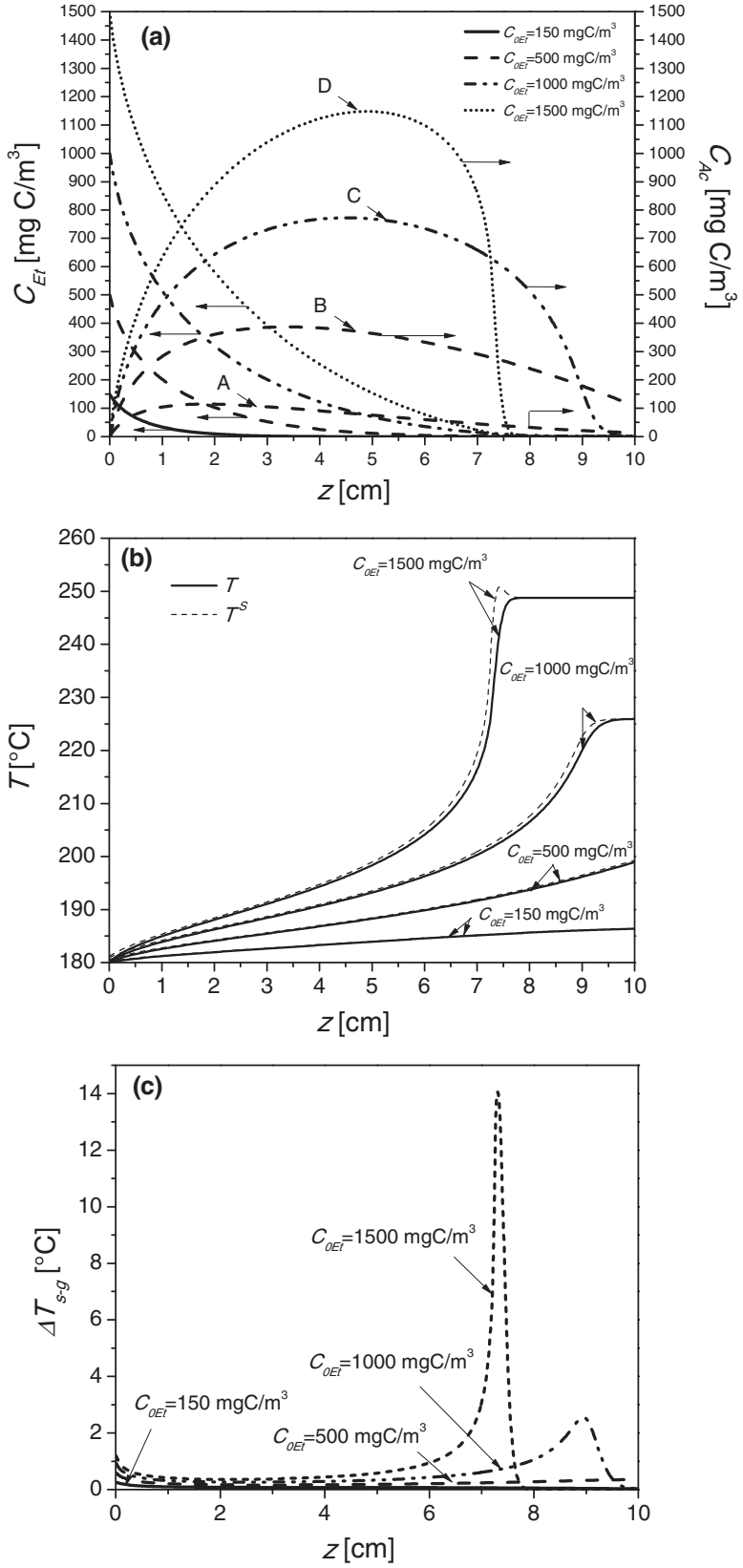

Fig. 5. (a) Axial concentration profiles of ethanol and acetaldehyde, (b) axial temperatures profiles in the gas (continuous line) and solid (dashed lines) phases, (c) axial profiles of temperature drop over the film, for the four operating conditions shows in Fig. 4.

Both models overlap at low C_{0Et} values, for which the thermal effects are low. In the case of the adiabatic model, a maximum in the $T_{0,min}$ curve there exists, i.e, $(T_{0,min})_{max}$, above which the monolithic reactor should be operated to ensure the allowed VOC emission for the entire C_{0Et} range. For the isothermal conditions, continuous increases in $T_{0,min}$ with C_{0Et} would be necessary to meet

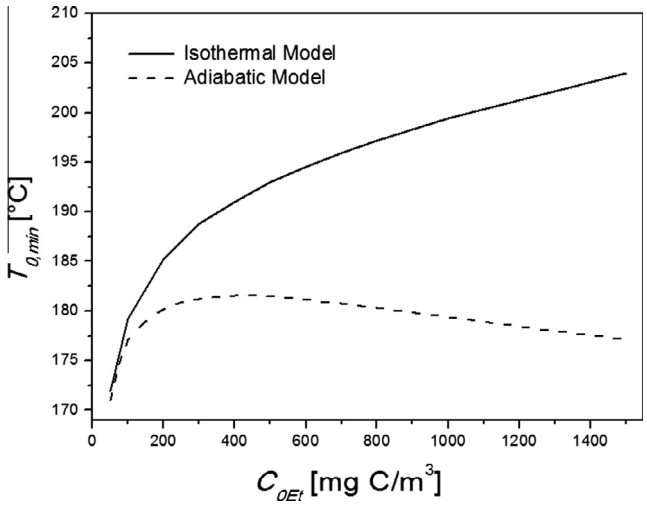

Fig. 6. $T_{0,min}$ for different C_{0Et}. Comparison between the adiabatic and the isothermal models for the conditions of Fig. 4.

VOC emissions specifications. However, this will not be the case when large scale monolithic reactors are being used for VOC abatement.

3.2. Influence of inlet flow rate (Q_0)

Fig. 7 shows the influence of the gas hourly space velocity on the values of $T_{0,min}$ by varying the inlet flow rate (Q_0). A reference value of Q_0^* = 37.2 Nm^3/h is considered (intermediate curve). As Q_0 increases, higher inlet temperatures are required, to satisfy the outlet specifications. This increase in the values of $T_{0,min}$ with Q_0 is necessary to compensate the lower residence times. Moreover, an additional amount of heat is required to achieve the energetic supply to preheat larger air streams.

Three different operative conditions are indicated in Fig. 7: points A, B and C, which are selected for a given value of C_{0Et} (1000 mg C/m^3) at different Q_0.

Fig. 8 exhibits the axial temperature profiles in the gas and solid phases for the three operative conditions specified above. In all the cases, the temperature profiles have a moderate increase of temperature in more than half of the reactor length, showing a steeper temperature elevation in the final zone of the reactor, where

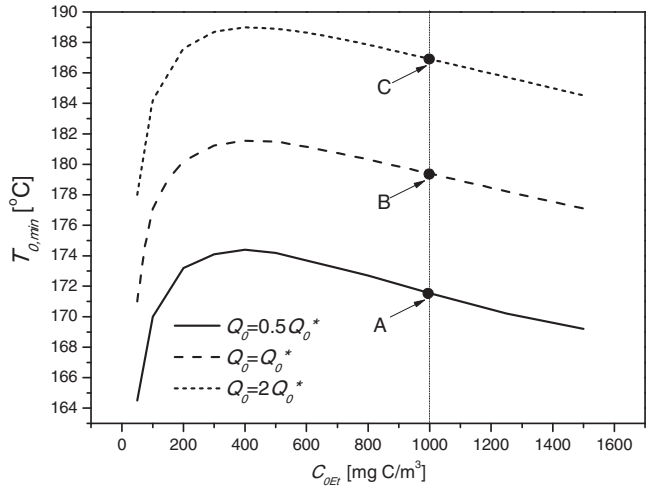

Fig. 7. $T_{0,min}$ for different C_{0Et}. Influence of inlet flow rate Q_0 for the condition of Fig. 4.

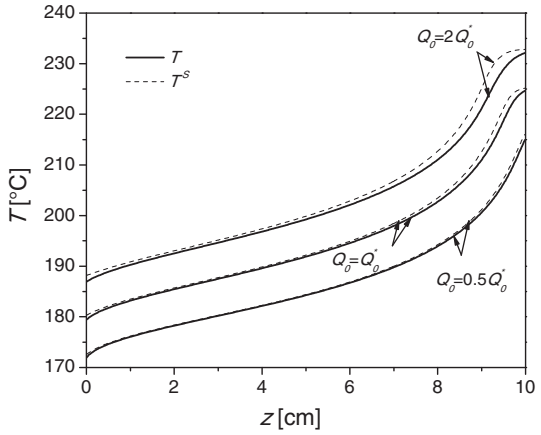

Fig. 8. Axial temperatures profiles in the gas (continuous line) and solid (dashed lines) phases for the operative conditions of Fig. 7 (points A, B and C).

mainly proceeds the acetaldehyde consumption by reaction 2, significantly more exothermic than reaction 1 (Table 2). The three temperature profiles for the gas phase are almost parallel, achieving a similar total temperature increase (~45 °C), due to the VOC concentrations at both reactor inlet (1000 mg C/m^3) and reactor outlet (20 mg C/m^3) are the same for all the cases. As Q_0 increases the temperature level in the reactor rises, this leads to faster effective reaction rates, i.e. higher heat generation rates. As a consequence, $\Delta T_{s\text{-}g}$ becomes more relevant. This is confirmed by inspection of the curves: the temperature profiles for both phases tend to separate as Q_0 increases.

Fig. 9a shows axial profiles of effective reaction rate 1 (left ordinate axis) for the operating conditions of Fig. 8. The r_1^{eff} profiles are descending in agreement with the ethanol depletion. As Q_0 increases r_1^{eff} is higher because of the higher $T_{0,min}$ required to meet the specifications. The internal effectiveness factors of reaction 1 ($\eta_{1,\text{int}}$), defined as the ratio between r_1^{eff} and r_1^S are presented in Fig. 9a (right ordinate axis). A non-monotonous behaviour is registered, with a climb in the first quarter of the reactor length, achieving then a plateau zone and finally a decrease in the last quarter of the reactor length. $\eta_{1,\text{int}}$ show the lower values in zones where acetaldehyde concentration is low. This behaviour is associated with the kinetic expression for reaction 1 (LHHW type) and the relative behaviour between r_1^{eff} and r_1^S in different axial positions inside the reactor. Non-monotonous behaviours in the effectiveness factors have been reported in the literature for LHHW kinetics expressions [16].The highest temperatures associated with the high flow rates tend to increment the mass transfer resistances in the washcoat and the lowest $\eta_{1,\text{int}}$ are found. Fig. 9b shows the corresponding axial profiles of effective reaction rate 2 (left ordinate axis). The r_2^{eff} profiles present a maximum in axial positions where acetaldehyde is mainly consumed. As expected, for higher Q_0, the temperatures inside the reactor are higher (see Fig. 8), this leads to faster reaction rates and the maximum values of r_2^{eff} are found when Q_0 increases. The internal effectiveness factor of reaction 2 ($\eta_{2,\text{int}}$) is also included in Fig. 9b; $\eta_{2,\text{int}}$ is defined as the ratio between r_2^{eff} and r_2^S. In the first zone of the reactor, where acetaldehyde is mainly generated, $\eta_{2,\text{int}}$ is higher than 1. Conversely, in the last zone of the reactor where acetaldehyde is mainly consumed $\eta_{2,\text{int}}$ is lower than 1. This drop is more pronounced at high Q_0 values, since the reactor operates at high temperatures levels and internal mass transfer resistances become more relevant. In the middle of the reactor, $\eta_{2,\text{int}}$ present a plateau zone with a value close to 1. Again, when acetaldehyde concentration is low, reaction

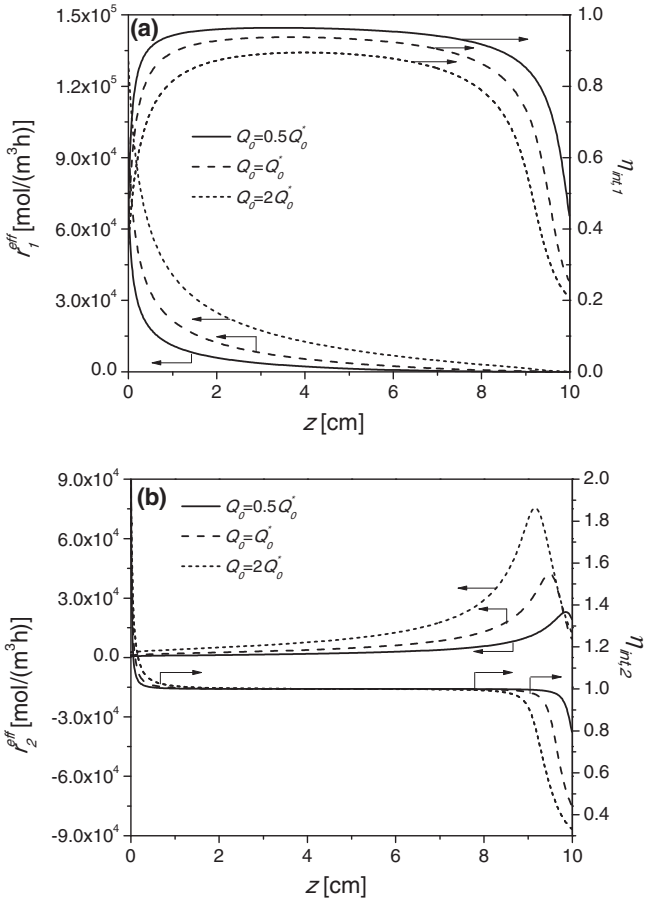

Fig. 9. (a) Axial profiles of effective reaction rate 1 (r_1^{eff}) and internal effectiveness factor of reaction 1 ($\eta_{1,int}$), (b) axial profiles of effective reaction rate 2 (r_2^{eff}) and internal effectiveness factor of reaction 2 ($\eta_{2,int}$), for the operative conditions selected in Fig. 7 (points A, B and C).

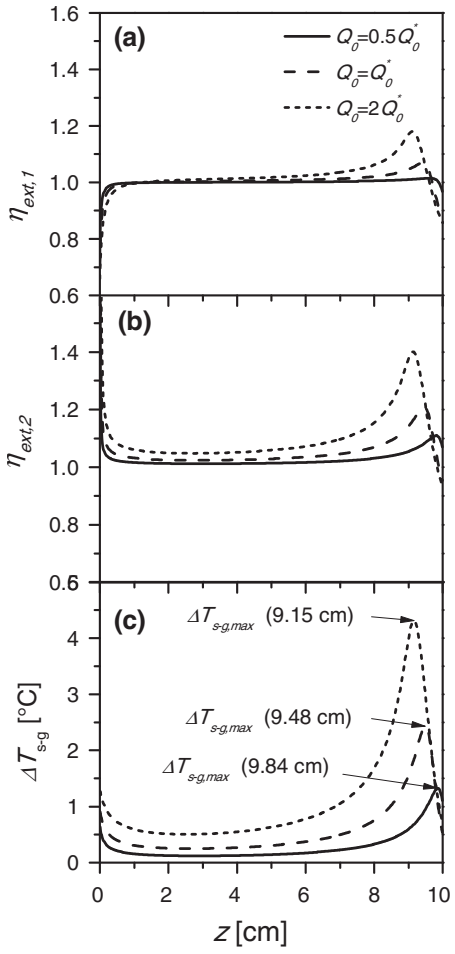

Fig. 10. (a) Axial profiles of external effectiveness factor of reaction 1 ($\eta_{1,ext}$), (b) axial profiles of external effectiveness factor of reaction 2 ($\eta_{2,ext}$) and (c) axial profiles of temperature drop over the film, for the operating conditions selected in Fig. 7 (points A, B and C).

2 behaves as a first order reaction (see Eq. (2)) and $\eta_{2,int}$ takes values different to one. In zones where acetaldehyde concentration is high enough, reaction 2 approximates to a zero order reaction and $\eta_{2,int} \sim 1$.

Fig. 10 displays the external effectiveness factors of reaction 1 (Fig. 10a), external effectiveness factor of reaction 2 (Fig. 10b), as well as interfacial temperatures gradients (Fig. 10c), for the operative conditions selected in Fig. 7 (points A, B and C). $\eta_{i,ext}$ is defined as the ratio between r_i^S and r_i^B. As it can be observed, $\eta_{1,ext}$ and $\eta_{2,ext}$ exceed the unity in axial positions where the temperature drop over the film achieves their maximum value. This behaviour is favoured at high Q_0. In these situations, the heat generation rate is higher and, as a consequence, the maximum temperature drop over the film increases and its axial position shifts to the entrance (from z = 9.84 cm to 9.15 cm, see Fig. 10c).

The axial position where $\Delta T_{s-g,max}$ are located coincide not only with the maximum slopes in the gas-phase axial temperature profiles (see Fig. 8), but also with the position where r_2^{eff} achieved their maximums values (see Fig. 9b). Notice that heat of reaction 2 is clearly higher than heat of reaction 1 ($\Delta Hr_2 > \Delta Hr_1$).

For the highest flow rate considered ($Q_0 = 2Q_0^*$), at axial positions where $\Delta T_{s-g,max}$ is located r_1^S is almost 20% greater than r_1^B (Fig. 10a) and r_2^S is 40% superior than r_2^B (Fig. 10b). This higher sensibility of r_2 with temperature finds its explanation in the activation energy values ($E_2 > E_1$, see Table 2).

Fig. 11 shows ΔT_{s-g} vs. the heat generation rates (q_{gen}) defined as the right hand side of Eq. (12)), for the operating conditions

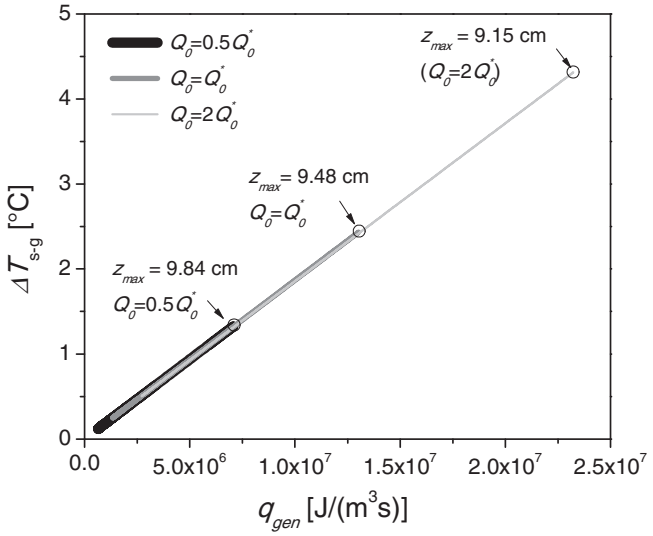

Fig. 11. Temperature drop over the film vs. heat generation rates for the operating conditions selected in Fig. 7 (points A, B and C).

indicated in Fig. 7. As it can be observed, the three cases are situated over a same straight line, which slope is defined as the inverse

of the product $a_v h_e$ (see Eq. (12)). The slope is nearly the same in the three cases due to h_e has a slight dependence with u_s (Q_0) and the interfacial area remains unchanged (e.g. the same design parameters are considered).

However, the heat generation increases with Q_0 due to the fact that higher temperatures are required to eliminate the increasing molar flows of VOC fed to the monolith. While ΔT is the same in all the cases, increasing $\Delta T_{s\text{-}g}$ are needed to transfer the heat generated from the solid phase. The maximum heat generation are located at axial positions where the $\Delta T_{s\text{-}g,max}$ are found, these positions are indicated on Fig. 11.

Fig. 12a displays concentration cross-section profiles of ethanol and acetaldehyde at the reactor inlet (z = 0 cm). As expected, the ethanol profiles decrease along the x coordinate, while acetaldehyde profiles increase with x, because of the prevalence of the generation rate (r_1). As Q_0 increases, external and internal concentration gradients for ethanol and acetaldehyde are more pronounced due to the fact that higher $T_{0,min}$ are needed.

Fig. 12b shows concentration cross-section profiles of ethanol and acetaldehyde at an axial position near the reactor outlet (z = 9.5 cm). At this axial position, ethanol is almost depleted and prevails acetaldehyde consumption due to decreasing concentration cross-section profiles of the intermediary are observed. As Q_0 increases, it is necessary eliminate higher molar flows of VOCs. As a consequence, steeper external and internal concentration cross-section profiles of ethanol and acetaldehyde are detected.

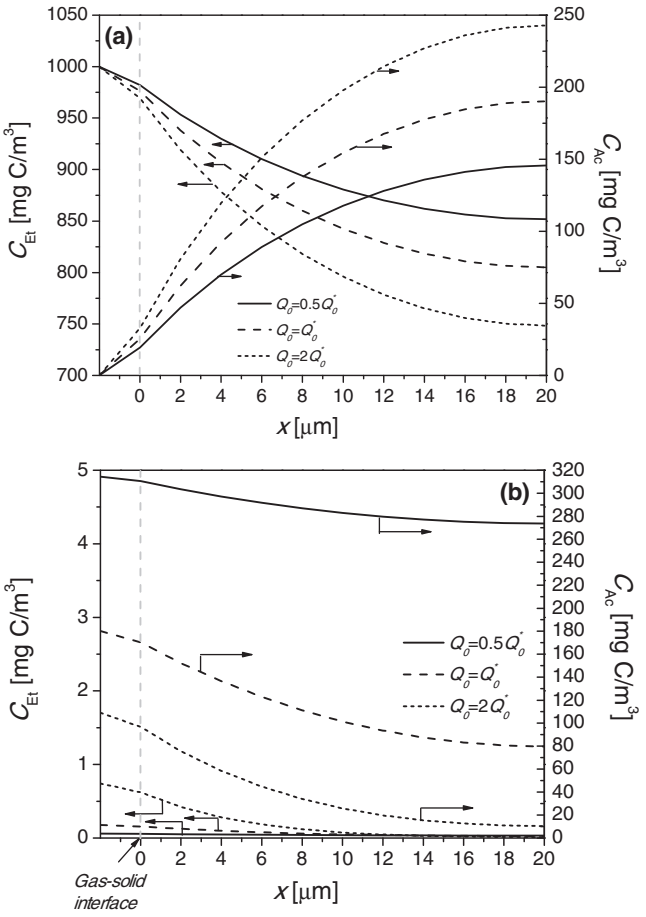

Fig. 12. (a) Concentration cross-section profiles of ethanol (left ordinate axis) and acetaldehyde (first right ordinate axis) in the gas phase and the washcoat at the reactor inlet (z = 0 cm). (b) Concentration cross-section profiles of ethanol (left ordinate axis) and acetaldehyde (first right ordinate axis) at an axial position near the reactor outlet (z = 9.5 cm), for the operating conditions selected in Fig. 7 (points A, B and C).

3.3. Influence of design parameters on the reactor performance

3.3.1. Influence of washcoat thickness (δ_w)

To analyse the effect of washcoat thickness, this geometrical parameter is increased from its reference value, δ_w = 20 μm, up to δ_w = 80 μm. The remaining parameters are kept constant (b = 1.5 mm, CN = 13,950, L = 10 cm). The results are obtained at constant ethanol inlet concentration (C_{0Et} = 1000 mg C/m^3), constant inlet temperature (T_0 = 178 °C) and constant space velocity ($GHSV$ = 2.61 × 10^5 1/h). To maintain constant the space velocity, Q_0 is increased as δ_w rises. Table 4 shows the geometrical parameters and operative conditions that have been modified for each thickness value. Table 5 lists Reynolds numbers and convective mass and heat transfer coefficients for each case.

Fig. 13 shows the outlet VOC concentration (C_{VOC}) for different washcoat thickness for both models, adiabatic heterogeneous and adiabatic pseudohomogeneous models.

In the case of the pseudohomogeneous model the internal and external mass transport resistances and the interfacial temperature gradients have been neglected, consequently the effectiveness factors in the mass and heat balances of gas phase are set equal to 1 (see Eqs. (3)–(7)).

For the heterogeneous model, it can be observed that C_{VOC} increases with δ_w. When the washcoat thickness (δ_w) is over 42 μm, VOC emissions exceed the allowable value (C^*_{VOC} = 20 mg C/m^3). As a result of the low evolution of the reaction rates (low VOC outlet conversion), the total heat generation is lower and the reactor temperature rise decrease (see the curve corresponding to ΔT).

The internal effectiveness factors for both reactions, $\overline{\eta}_{1,\text{int}}$ and $\overline{\eta}_{2,\text{int}}$ (axially averaged values) tend to decrease with δ_w, which is consistent with the increment of the internal mass transfer resistances for reactions 1 and 2. Notice in the case of $\overline{\eta}_{1,\text{int}}$ this drop is more pronounced than in the case of $\overline{\eta}_{2,\text{int}}$. As it was shown previously, in Fig. 9b, $\eta_{2,\text{int}}$ remains close to one in a wide zone of the reactor, as a consequence $\overline{\eta}_{2,\text{int}}$ is slightly lower than 1.

The axially averaged external effectiveness factors, $\overline{\eta}_{1,ext}$ and $\overline{\eta}_{2,ext}$, show a slight increase with δ_w, which is in accordance with the loss in the interfacial area (a_v) (see Table 4). That is, lower

Table 4
Geometrical parameter and operative conditions for the conditions of Fig. 13.

Washcoat thickness (δ_w) [m]	Open frontal area (A_o) [m^2]	Washcoat volume (V_w) [m^3]	Washcoat mass (m_w) [kg]	Inlet flow rate (Q_0) [Nm^3/h]	Linear velocity (u_s) [m/s]	Interfacial area (a_v) [m^2/m^3]
20 × 10^{-6}	0.0297	1.65 × 10^4	0.6656	43.20	0.4036	4.932 × 10^4
30 × 10^{-6}	0.0289	2.46 × 10^4	0.9917	64.36	0.6181	3.265 × 10^4
40 × 10^{-6}	0.0281	3.26 × 10^4	1.3133	85.23	0.8417	2.432 × 10^4
50 × 10^{-6}	0.0273	4.05 × 10^4	1.6303	105.81	1.0750	1.931 × 10^4
60 × 10^{-6}	0.0266	4.82 × 10^4	1.9429	126.10	1.3185	1.597 × 10^4
70 × 10^{-6}	0.0258	5.59 × 10^4	2.2510	146.09	1.5728	1.359 × 10^4
80 × 10^{-6}	0.0250	6.34 × 10^4	2.5546	165.79	1.8386	1.180 × 10^4

Table 5
Reynolds numbers and convective mass and heat transfer coefficients for the conditions of Fig. 13.

Washcoat thickness (δ_w) [m]	Re	Convective mass transfer coefficient kg_1 [m/s]	Convective mass transfer coefficient kg_2 [m/s]	Convective heat transfer coefficient he [J/(s m^2 K)]
20×10^{-6}	18.43	0.58	0.58	80.36
30×10^{-6}	27.83	0.59	0.59	81.76
40×10^{-6}	37.38	0.60	0.60	83.21
50×10^{-6}	47.07	0.61	0.61	84.68
60×10^{-6}	56.93	0.62	0.62	86.20
70×10^{-6}	66.96	0.63	0.63	87.75
80×10^{-6}	77.17	0.64	0.64	89.35

interfacial areas lead to higher interfacial temperature differences and, consequently, to higher external effectiveness factors. It is important to note that despite the external effectiveness factors show an opposite behaviour respect internal effectiveness factors, the last effect predominates and governs the process: the performance of the monolithic reactor deteriorates with the increase in the washcoat thickness.

Fig. 13 also reveals that according to the predictions of the pseudohomogeneos model, for the operating conditions selected, VOCs would be completely removed ($C_{VOC} \sim 0$) independently of the washcoat thickness considered. This model performs a non-realistic representation of the reactor performance with a clear overestimation of VOC conversions, which is more evident as δ_w increases.

3.3.2. Influence of channel width (b)

To analyse the effect of channel width (b), this geometrical parameter is increased from 0.5 mm to 2.4 mm. With this purpose the ethanol inlet concentration (C_{0Et} = 1000 mg C/m^3), the inlet temperature (T_0 = 180 °C), the inlet flow rate (Q_0) and the gas hourly space velocity ($GHSV$ = 3.31 × 10^5 1/h) are maintained constant. For all the cases analysed, the total transversal area (A_T = 0.01734 m^2) is also maintained invariant. As b increases, δ_w and CN are jointly adjusted to keep constant the space velocity (see Table 6). The rest of the design parameters remain unchanged (see Table 3).

Table 6
Geometrical parameter and operative conditions for the conditions of Fig. 14.

Channel width (b) [m]	Channel number (CN) [adim]	Washcoat thickness (δ_w) [m]	Interfacial area (a_v) [m^2/m^3]	Lateral area (A_l) [m]
0.250×10^{-3}	277,388	4.40×10^{-6}	21.900×10^4	26.80
0.500×10^{-3}	69,347	8.81×10^{-6}	10.950×10^4	13.40
1.115×10^{-3}	13,950	20.00×10^{-6}	4.912×10^4	6.00
1.500×10^{-3}	7705	26.40×10^{-6}	3.651×10^4	4.46
2.000×10^{-3}	4334	35.20×10^{-6}	2.738×10^4	3.35
2.400×10^{-3}	3010	42.30×10^{-6}	2.282×10^4	2.79

As b is increased, a noticeable loss in lateral (interfacial) area occurs, as a consequence of both, the decrease in the channel number and the increase in the washcoat thickness. Fig. 14 illustrates that higher washcoat thickness lead to drops in the averaged internal effectiveness factors, $\overline{\eta}_{1,\text{int}}$ and $\overline{\eta}_{2,\text{int}}$. As explained before, $\overline{\eta}_{2,\text{int}}$ is less affected than $\overline{\eta}_{1,\text{int}}$ by the increase in washcoat thickness.

Moreover, the loss in the interfacial area causes an increase in the interfacial temperature gradient and the averaged external effectiveness factors $\overline{\eta}_{1,ext}$ and $\overline{\eta}_{2,ext}$ become higher than one. This effect is confirmed by the increase in the maximum gas-solid temperature ($\Delta T_{s\text{-}g,max}$) as it is indicated in the second right ordinate axis of Fig. 14. The higher sensibility of $\overline{\eta}_{2,ext}$ than $\overline{\eta}_{1,ext}$ with the loss in the interfacial area (higher b) finds its explanation in the activation energy values of each reaction ($E_2 > E_1$).

Despite both effect are opposite, the external thermal resistances control the process and lower VOC outlet concentrations are achieved as the channel width is enlarged.

Under these conditions, the pseudohomogeneous model predicts an invariant C_{VOC} at the reactor outlet. Conversely to the results show in Fig. 13, in this case neglecting the transport resistances lead to underestimate the VOC conversions. Except for the smallest channels, the differences in the predictions between both models are significant.

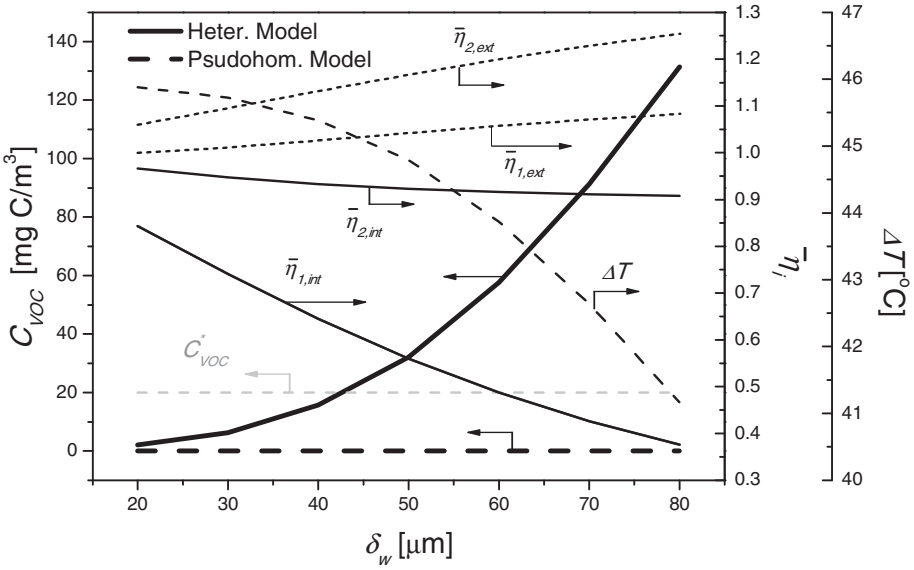

Fig. 13. Outlet VOC concentration (C_{VOC}) for heterogeneous and pseudohomogeneos models (left ordinate axis), internal and external effectiveness factor for reactions r_1 y r_2 (first right ordinate axis) and total temperature gradient in gas phase (second right ordinate axis) for b = 1.5 mm, CN = 13950, L = 10 cm, C_{0Et} = 1000 mg C/m^3, T_0 = 178 °C and $GHSV$ = 2.61 × 10^5 1/h.

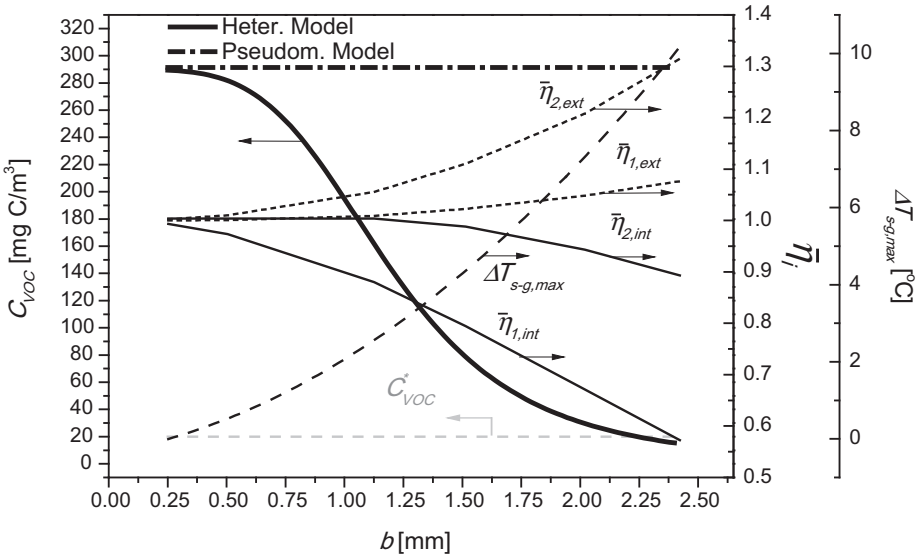

Fig. 14. Outlet VOC concentration (C_{VOC}) for heterogeneous and pseudohomogeneous models (left ordinate axis), internal and external effectiveness factor for reactions r_1 y r_2 (first right ordinate axis) and maximum gas-solid temperature (second right ordinate axis) L = 10 cm, C_{0Et} = 1000 mg C/m^3, T_0 = 180 °C and $GHSV = 3.31 \times 10^5$ 1/h.

4. Conclusions

From the previous results, the following main conclusions can be summarized:

The minimum inlet temperature becomes a key parameter to control and ensure environmental standards of VOC emissions with low energy requirements are met, for different total gas flow rates and inlet VOC concentrations. At high values of C_{0Et} the heat effects are greater and lower inlet temperatures are needed to achieve C^*_{VOC}, i.e., for an increase of 1000 mg C/m^3 in the inlet ethanol concentration (from 500 to 1500 mg C/m^3), the decrease in $T_{0,min}$ is around 5 °C. The interfacial thermal gradient rises up to 12 °C for the higher C_{0Et}.

As Q_0 increases, higher $T_{0,min}$ are required, r_1^{eff} and r_2^{eff} increase leading to more pronounced concentration gradients of ethanol and acetaldehyde inside de washcoat. As a consequence, axially average internal effectiveness factors $\overline{\eta}_{1,\text{int}}$ and $\overline{\eta}_{2,\text{int}}$ diminish.

A diminution of the interfacial area of the monolithic reactor result a key design parameter to achieve the consumption of VOCs. As the channel width is increased, less interfacial area is available to deposit the catalyst. If the washcoat thickness is increased in order to maintain the total catalyst mass constant, lower internal effectiveness factors are found. However, the loss in gas-solid area amplifies the interfacial temperature gradients. These external temperature gradients overcompensates the adverse effect of the internal mass transfer resistances. Consequently, the VOC abatement is favoured for the wider channels.

Notice that opposite conclusions can be obtained for lower values of ethanol feed concentrations. In fact, as ethanol inlet concentration decreases, heat effects become less relevant, the influence of the internal mass transfer resistances prevails and the smallest values of channel width arise as the most convenient.

The washcoat thickness increase for a given channel width leads to a loss in the interfacial area, and, consequently, to higher interfacial temperature differences and higher external effectiveness factors. Despite the external effectiveness factors show an opposite behaviour respect internal effectiveness factors, the last effect predominates and governs the process. When the washcoat thickness (δ_w) is over 42 μm, $\overline{\eta}_{1,\text{int}}$ is lower than 0.63 and $\overline{\eta}_{2,\text{int}}$ is lower than 0.93 for the conditions tested and VOC emissions exceed the allowable value (C^*_{VOC} = 20 mg C/m^3).

Finally, it is important to remark the need of taking into account the influence of the mass and heat transport resistances on the reactor performance. Depending on the selected conditions, pseudohomogeneous models can significantly over- or underestimate the outlet VOC concentration, leading respectively, to undesirable situations of excessive preheating of the air stream to meet VOC emissions specifications or, conversely, to risky conditions of incomplete VOC abatement.

Acknowledgements

Support of this work through Universidad Nacional de San Luis (UNSL), Universidad Nacional del Sur (UNS), Agencia Nacional de Promoción Científica y Tecnológica (ANPCyT) and Consejo Nacional de Investigaciones Científicas y Tecnológicas (CONICET) is fully acknowledged.

References

[1] K. Everaert, J. Baeyens, Catalytic combustion of volatile organic compounds, J. Hazard. Mater. B109 (2004) 113–119.
[2] European Commission. <http://ec.europa.eu/environment/air/legis.htm> (last access: 03/12/2015).
[3] T. Mitsui, T. Matsui, R. Kikuchi, K. Eguchi, Low-temperature complete oxidation of ethyl acetate over CeO_2-supported precious metal catalysts, Top. Catal. 52 (2009) 464–469.
[4] G. Ertl, H. Knözinger, F. Schüth, J. Weitkamp, Handbook of Heterogeneous Catalysis, second ed., Wiley-VCH, Weinheim, 2008.
[5] T.V. Choudhary, S. Banerjee, V.R. Choudhary, Catalysts for combustion of methane and lower alkanes, Appl. Catal. A 234 (2002) 1–23.
[6] W.B. Li, J.X. Wang, H. Gong, Catalytic combustion of VOCs on non-noble metal catalysts, Catal. Today 148 (2009) 81–87.
[7] M.R. Morales, B.P. Barbero, L.E. Cadús, Evaluation and characterization of Mn–Cu mixed oxide catalysts for ethanol total oxidation: Influence of copper content, Fuel 87 (2008) 1177–1186.
[8] Haden Drysys International, Thermal oxidation and other VOC abatement techniques, Filtr. Sep. 34 (1997) 324–325. and 327–329.
[9] G. Baldissone, D. Fissore, M. Demichela, Catalytic after-treatment of lean VOC-air streams: process intensification vs. plant reliability, Process Saf. Environ. 100 (2016) 208–219.
[10] R. Litto, T. Nien, R.E. Hayes, J.P. Mmbaga, M. Votsmeier, Parametric study of a recuperative catalytic converter, Catal. Today 188 (2012) 106–112.
[11] R.M. Heck, S. Gulati, R.J. Farrauto, The application of monoliths for gas phase catalytic reactions, Chem. Eng. J. 82 (2001) 149.
[12] V. Tomasic, F. Jovic, State of the art in the monolithic catalysts/reactors, Appl. Catal. A 311 (2006) 112–121.

[13] P. Avila, M. Montes, E.E. Miró, Monolithic reactors for environmental applications: a review on preparation technologies, Chem. Eng. J. 109 (2005) 11–36.
[14] J. Chen, H. Yang, N. Wanga, Z. Ring, T. Dabros, Mathematical modeling of monolith catalysts and reactors for gas phase reactions, Appl. Catal. A 345 (2008) 1–11.
[15] S.T. Kolaczkowski, S. Serbetcioglu, Development of combustion catalysts for monolith reactors: a consideration of transport limitations, Appl. Catal. A: Gen. 138 (1996) 199–214.
[16] R.E. Hayes, S.T. Kolaczkowski, Introduction to Catalytic Combustion, first ed., Gordon and Breach Science Publishers, Netherlands, 1997.
[17] S.T. Kolaczkowski, Modelling catalytic combustion in monolith reactors – challenges faced, Catal. Today 47 (1999) 209–218.
[18] R.E. Hayes, S.T. Kolaczkowski, Mass and heat transfer effects in catalytic monolith reactors, Chem. Eng. Sci. 49 (1994) 3587–3599.
[19] D. Leung, R.E. Hayes, S.T. Kolaczkowski, Diffusion limitation in the washcoat of a catalytic monolith reactor, Can. J. Chem. Eng. 74 (1996) 94–103.
[20] V. Tomašić, Z. Gomzi, Experimental and theoretical study of NO decomposition in a catalytic monolith reactor, Chem. Eng. Proc. 43 (2004) 765–774.
[21] R.E. Hayes, B. Liu, R. Moxom, M. Votsmeier, The effect of washcoat geometry on mass transfer in monolith reactors, Chem. Eng. Sci. 59 (2004) 3169–3181.
[22] A. Holmgren, B. Andersson, Mass transfer in monolith catalysts–CO oxidation experiments and simulations, Chem. Eng. Sci. 53 (1998) 2285–2298.
[23] A. Kolodziej, J. Lojewska, Short-channel structured reactor for catalytic combustion: design and evaluation, Chem. Eng. Process. 46 (2007) 637–648.
[24] G. Groppi, E. Tronconi, P. Forzatti, Modelling of catalytic combustors for gas turbine applications, Catal. Today 17 (1993) 237–250.
[25] R.H. Heck, J. Wei, J.R. Katzer, Mathematical modelling of catalytic monoliths, AIChE J. 22 (1976) 477–484.
[26] L.C. Young, B.A. Finlayson, Mathematical model of the monolithic converter. Part I. Development of model and application of orthogonal collocation, AIChE 22 (1976) 343–353.
[27] F.N. Agüero, M.R. Morales, F. Duran, B.P. Barbero, L.E. Cadús, MnCu/cordierite monolith used for catalytic combustion of volatile organic compounds, Chem. Eng. Technol. 36 (2013) 1749–1754.
[28] A. Cybulski, J.A. Moulijn, Monoliths in heterogeneous catalysis, Catal. Rev. 36 (1994) 179–270.
[29] F.P. Incropera, D.P. DeWitt, T.L. Bergman, A.S. Lavine, Fundamental of Heat and Mass Transfer, Wiley and Sons, 2001, p. 260.
[30] F. Kapteijn, G.B. Marin, J.A. Moulijn, Catalytic reaction engineering, Chapter 8 in catalysis: an integrated approach, in: R.A. van Santen, P.W.N.M. van Leeuwen, J.A. Moulijn, B.A. Averill (Eds.), Elsevier, Amsterdam, 1999, p. 408.
[31] M.A. Campesi, N.J. Mariani, M.C. Pramparo, B.P. Barbero, L.E. Cadús, O.M. Martínez, G.F. Barreto, Combustion of volatile organic compounds on a MnCu catalyst: a kinetic study, Catal. Today 176 (2011) 225.
[32] J.M. Smith, H.C. Van Ness, M.M. Abbott, Introduction to Chemical Engineering Thermodynamics, McGraw-Hill, New York, 2005.
[33] M.A. Campesi, Estudio de sistemas combinados de combustión catalítica de VOCs PhD Thesis, Universidad Nacional de La Plata, Argentina, 2012. http://sedici.unlp.edu.ar/bitstream/handle/10915/27082/Documento_completo.pdf?sequence=1.
[34] R.C. Reid, J.M. Prausnitz, T.K. Sherwood, The Properties of Gases and Liquids, third ed., Mc Graw Hill, New York, 1977.
[35] R.D. Hawthorn, Afterburner catalysis—effects of heat and mass transfer between gas and catalyst surface, AIChE Symp. Ser. 70 (1974) 428–438.
[36] E.N. Fuller, P.D. Schettler, J.C. Giddings, New method for prediction of binary gas-phase diffusion coefficients, Ind. Eng. Chem. 58 (1966) 19–27.
[37] G.F. Froment, K.B. Bischoff, Chemical Reactor Analysis and Design, second ed., Wiley, Toronto, Canada, 1990.
[38] L.F. Shampine, C.W. Gear, A users view of solving stiff ordinary differential equations, SIAM Rev. 21 (1979) 1–17.